NANOMATERIALS

Tunable porous nanoallotropes prepared by post-assembly etching of binary nanoparticle superlattices

Thumu Udayabhaskararao,[1] Thomas Altantzis,[2] Lothar Houben,[3,4] Marc Coronado-Puchau,[5] Judith Langer,[5,6] Ronit Popovitz-Biro,[3] Luis M. Liz-Marzán,[5,6,7] Lela Vuković,[8] Petr Král,[9,10,11] Sara Bals,[2] Rafal Klajn[1]*

Self-assembly of inorganic nanoparticles has been used to prepare hundreds of different colloidal crystals, but almost invariably with the restriction that the particles must be densely packed. Here, we show that non–close-packed nanoparticle arrays can be fabricated through the selective removal of one of two components comprising binary nanoparticle superlattices. First, a variety of binary nanoparticle superlattices were prepared at the liquid-air interface, including several arrangements that were previously unknown. Molecular dynamics simulations revealed the particular role of the liquid in templating the formation of superlattices not achievable through self-assembly in bulk solution. Second, upon stabilization, all of these binary superlattices could be transformed into distinct "nanoallotropes"—nanoporous materials having the same chemical composition but differing in their nanoscale architectures.

Self-assembly has emerged as the strategy of choice toward generating ordered arrays of nanosized particles. The resulting materials—in particular, those assembled from inorganic nanoparticles (NPs) (*1*–*7*)—often exhibit unanticipated optical (*8*), thermoelectric (*9*), magnetic (*10*), catalytic (*11*), and other (*12*) properties. The diversity of structures and presumably the properties of these materials could be greatly enhanced via postsynthetic modifications, which could be used to generate assemblies in which the constituent NPs are ordered yet separated by relatively large distances—that is, non–close-packed (NCP) NP arrays. Although several examples of related materials have been reported, they are limited to highly specific systems, such as those involving highly directional interactions (*13*, *14*) or a fine balance between attractive and repulsive forces during self-assembly (*15*). Thus, a general route to NCP NP arrays has been lacking.

One strategy to tackle this limitation could be based on the selective removal (by means of chemical etching) of one type of NPs from binary NP superlattices (BNSLs) (*1*). Depending on the stoichiometry and structure of the initial BNSLs, this method could lead to "nanoallotropes"—materials that have the same chemical composition but differ in their nanoscale architecture. Unfortunately, within BNSLs the two types of nanoscopic components mutually support each other, and removal of one would inevitably lead to the disruption of the other. Here, we hypothesized that this undesired behavior could be overcome by stabilizing the BNSL through controlled removal of the surfactants from the NP surfaces (*16*–*18*). If successful, this procedure would serve three purposes: (i) attaching the NPs to the underlying surface, (ii) controlling the coalescence of the NPs, and (iii) activating the sacrificial component of the BNSL toward etching.

We worked with monodisperse batches of Au and Fe_3O_4 NPs (figs. S1 and S2) (*19*), which we assembled at the diethylene glycol (DEG)–air interface (Fig. 1A, step 1), as previously reported (*20*). After transfer onto a carbon-coated transmission electron microscopy (TEM) copper grid (Fig. 1A, step 2) and a controlled, thermally induced desorption of ligands from the NPs (Fig. 1A, step 3) (*17*), the samples were exposed to an etchant reacting with only one of the two materials (Fig. 1A, step 4). As a proof of concept, we co-assembled a ~1:1 mixture of 5.2 (±0.4) nm dodecanethiol-protected Au NPs and 10.6 (±0.6) nm oleate-protected Fe_3O_4 NPs into the previously reported (*20*) AB-type binary NP monolayer (Fig. 1B and figs. S3 to S6) (*19*). After immobilization onto carbon-coated TEM grids, Fe_3O_4 NPs could be etched out by immersing the substrate into an aqueous solution of HCl, without affecting the order of the gold NPs (Fig. 1C). For example, shown in Fig. 1E is an ensemble of 250 gold NPs, the positions of which all remained unaffected after HCl etching (figs. S7 and S8) (*19*). We will refer to the resulting NCP array of Au NPs as vac_1Au_1, where *vac* denotes "vacancy." Alternatively, a square array of self-supporting Fe_3O_4 NPs could be obtained by treating the BNSLs with a cyanide solution, which can selectively dissolve Au NPs (Fig. 1D).

The underlying substrate had a profound effect on the successful fixation of the NPs. The NPs could be readily immobilized on commercial carbon-coated Formvar films as well as on homemade carbon-coated nitrocellulose substrates. However, we found no attachment onto silicon wafers or nitrocellulose that lacked a layer of amorphous carbon (fig. S9) (*19*). From these results, we conclude that amorphous carbon facilitated the desorption of organic ligands from the NP surfaces and the formation of a carbonaceous film (*21*), which can serve as an adhesive for the NPs. The carbonaceous films can be directly visualized with TEM (fig. S10) (*19*). Overall, the above procedure allowed for the fabrication of NCP NP superlattices on thin, flexible substrates (Fig. 1C, inset), which could subsequently be transferred onto surfaces of choice.

Self-assembly from a ~5:1 mixture of Au and Fe_3O_4 NPs resulted in a different type of BNSL, as shown in Fig. 2A (fig. S11) (*19*). This array, featuring alternating clusters of Au NPs and individual Fe_3O_4 NPs, is akin to the previously reported Fe_4C-type BNSL (*22*). However, selective removal of the Fe_3O_4 counterpart allowed us to observe quintets—rather than quartets—of Au NPs arranged in a tetrahedral geometry (Fig. 2B and fig. S12) (*19*). To decipher the structure of this and other more complex assemblies, we conducted electron tomography studies (*23*, *24*) by acquiring series of two-dimensional (2D) projections of the etched arrays over a wide range of tilt angles using high-angle annular dark-field scanning transmission electron microscopy (HAADF-STEM). These studies confirmed that each cluster was composed of five Au NPs (giving rise to stoichiometry vac_1Au_5) (figs. S13 to S15) (*19*), and they helped elucidate the mutual packing of the resulting tetrahedra (Fig. 2, C and D, and database S1, tomography data) (*19*). The high stability of these tetrahedra could be attributed to partial coalescence of Au NPs, which occurred as a result of ligand desorption (*16*–*18*). As shown in the structural model in fig. S16, the vac_1Au_5 array is derived from an incomplete (deficient in Au) AB_6-type BNSL (*19*).

Our method allowed us to control the degree of coalescence by adjusting the time of thermal treatment; extending the heating time from 30 min to 6 hours allowed us to convert an ensemble of tetrahedra into a well-defined array of pseudospherical ~9-nm gold NPs (figs. S17 to S19) (*19*). An unexpected effect of heating was that Au NP quintets that lack a strong attachment to the underlying substrate could migrate and be transformed into well-defined sinuous nanowires (fig. S20) (*19*).

Increasing the Au:Fe_3O_4 NP ratio to ~10 led to another type of BNSL, which, after the removal

[1]Department of Organic Chemistry, Weizmann Institute of Science, Rehovot 76100, Israel. [2]EMAT, University of Antwerp, Groenenborgerlaan 171, B-2020 Antwerp, Belgium. [3]Department of Chemical Research Support, Weizmann Institute of Science, Rehovot 76100, Israel. [4]Ernst Ruska-Centre for Microscopy and Spectroscopy with Electrons, 52425 Jülich, Germany. [5]CIC BiomaGUNE, Paseo de Miramón 182, 20014 Donostia-San Sebastián, Spain. [6]Biomedical Research Networking Center in Bioengineering, Biomaterials, and Nanomedicine (CIBER-BBN), 20014 Donostia-San Sebastián, Spain. [7]Ikerbasque, Basque Foundation for Science, 48013 Bilbao, Spain. [8]Department of Chemistry, University of Texas at El Paso, El Paso, TX 79968, USA. [9]Department of Chemistry, University of Illinois at Chicago, Chicago, IL 60607, USA. [10]Department of Physics, University of Illinois at Chicago, Chicago, IL 60607, USA. [11]Department of Biopharmaceutical Sciences, University of Illinois at Chicago, Chicago, IL 60607, USA.
*Corresponding author. Email: rafal.klajn@weizmann.ac.il

Downloaded from http://science.sciencemag.org/ on October 26, 2017

of Fe_3O_4, exhibited features (Fig. 2, E and F, and figs. S21 to S23) (*19*) reminiscent of the previously reported (*25*) AB_{13}-type BNSL. The AB_{13}-type BNSL is composed of layers of quartets and quintets of the "B" NPs, following a $(\text{-}B_4\text{-}B_5\text{-}B_4\text{-})_n$ pattern. However, electron tomography studies on our etched material revealed that it consisted of alternating layers of NP quartets and septets [a $(\text{-}B_4\text{-}B_7\text{-})_n$ pattern] (Fig. 2, G and H), corresponding to an AB_{11} stoichiometry of the precursor BNSL (fig. S24, discussion) (*19*). Similar to the AB_6-type BNSLs, the AB_{11} arrays could be thermally transformed by partial sintering of the constituent Au NPs, resulting in nanoporous membranes (fig. S25, bottom) (*19*).

When the ratio of Au to Fe_3O_4 NPs was decreased to ~4 and a more polydisperse batch of Au NPs (4.9 ± 0.7 nm) was used, we observed the formation of BNSLs, within which the Au NPs were arranged into zigzag-like patterns (fig. S26) (*19*). Electron tomography analysis showed that this BNSL consisted of stacked NP layers having an AB_4 stoichiometry (Fig. 2I and figs. S27 to S29) (*19*), where "A" denotes a Fe_3O_4 NP and "B" denotes large, medium, and small Au NPs in a 1:2:1 ratio (for example, the NCP array shown in Fig. 2I consists of 6.2-, 5.3-, and 4.1-nm Au NPs). The fact that highly crystalline arrays could be assembled even from relatively polydisperse batches of NPs highlights the tendency of NPs to maximize the packing at the DEG-air interface. Analysis of the AB_4, AB_6, and AB_{11} BNSLs showed that they all share the same densely packed initial (bottom) monolayer [Fig. 2, D, H, and I, and figs. S16, S25, and S29, structural models (*19*)].

The formation of the above AB_4, AB_6, AB_{11}, and other structures not observed during self-assembly in three dimensions (bulk solution) suggests a profound effect of DEG on the assembly process (*26*, *27*). To disclose the mechanisms that govern self-assembly in our system, we performed precise atomistic molecular dynamics (MD) simulations of NPs at different liquid-air interfaces. These simulations, detailed in the supplementary materials, revealed that the role of DEG in guiding NP self-assembly is the result of a combination of several effects (*19*). First, the coupling energies of both types of NPs to DEG are large compared with the NP-NP coupling energies between exposed or partly submerged NPs (tables S1 and S2) (*19*). Hence, the NPs exhibit a high affinity to the surface of the underlying liquid, which they tend to cover in the most efficient way. Analysis of BNSLs assembled on the surface of DEG showed that as much as >50% of the lattice energies originates from NP-DEG, rather than NP-NP coupling (*19*). Second, both dodecanethiol-protected Au NPs and oleate-protected Fe_3O_4 NPs preferentially submerge in DEG to about half their diameter (Fig. 2, J to L). As a result, DEG can organize the bottom layer of NPs in a way that may not be achievable during self-assembly in bulk solution. Last, the coupling energy of the NPs to DEG per unit surface area of NP is approximately the same for both types of NPs. Thus, both Au and Fe_3O_4 NPs have a similar affinity toward the surface of DEG, from which they can displace each other during the self-assembly process. Taken together, these effects show that DEG can modify the free energies of BNSLs, favoring the formation of otherwise unstable BNSLs.

When the same polydisperse (4.9 ± 0.7 nm) Au and monodisperse 10.6 nm Fe_3O_4 NPs were used in a ~5:1 ratio, we observed the formation of an unprecedented quasi-ternary BNSL with a stoichiometry ABC_4, where "B" denotes a small (~4.0 nm) and "C" denotes a large (~5.5 nm) Au NP (fig. S30) (*19*). Subjecting this superlattice to our stabilization-etching procedure afforded a NCP $vac_1Au_1Au'_4$ array shown in Fig. 2, M to P (here, Au and Au′ denote small and large Au NPs, respectively) (figs. S31 to S34) (*19*). Within the ABC_4-type BNSL, the bottom-most Au and Fe_3O_4 NPs have their bottom boundaries (rather than the equatorial cross sections) at the same level. However, the "half-submergence condition" is still satisfied for both NP types if one considers the two 5.5-nm Au NPs placed on top of each other (in Fig. 2P, C and C′) as a single, elongated NP. Electron tomography studies could not resolve individual NPs within these putative dimers, suggesting that they undergo a partial coalescence (Fig. 2O, blue and red).

Our methodology could be extended to multilayers (figs. S35 to S43) (*19*), which is exemplified for a novel AB_4-type BNSL (Fig. 3A and figs. S40 and S44) (*19*). This BNSL was obtained

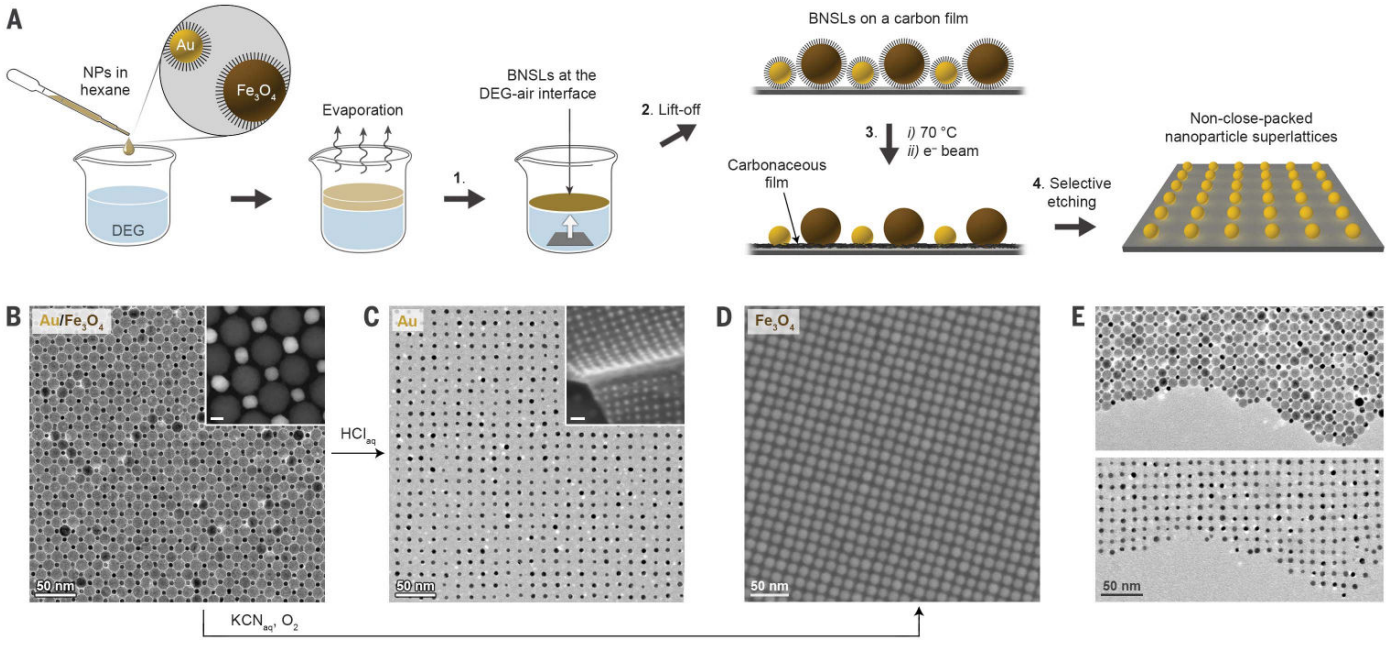


Fig. 1. Preparation of NCP nanoparticle arrays. (**A**) Schematic illustration of the method ("e⁻ beam" denotes an ~10 min exposure to the electron beam of a transmission electron microscope. (**B**) TEM image of an AB-type BNSL. The image in the inset was recorded in HAADF-STEM mode. Scale bar (inset), 5 nm. (**C**) TEM image of an NCP array of Au NPs (vac_1Au_1) obtained via selective removal of Fe_3O_4. (Inset) Scanning electron microscopy (SEM) image showing the flexible nature of the underlying film. Scale bar (inset), 20 nm. (**D**) SEM image of a NCP array of Fe_3O_4 NPs obtained via selective removal of Au [temperature below 70°C is not sufficient to remove the protective coating from the Fe_3O_4 NPs (*21*); the array remains stable because the relatively large Fe_3O_4 NPs mutually support one another]. (**E**) An edge of an AB-type BNSL before (top) and after (bottom) Fe_3O_4 etching.

Downloaded from http://science.sciencemag.org/ on October 26, 2017

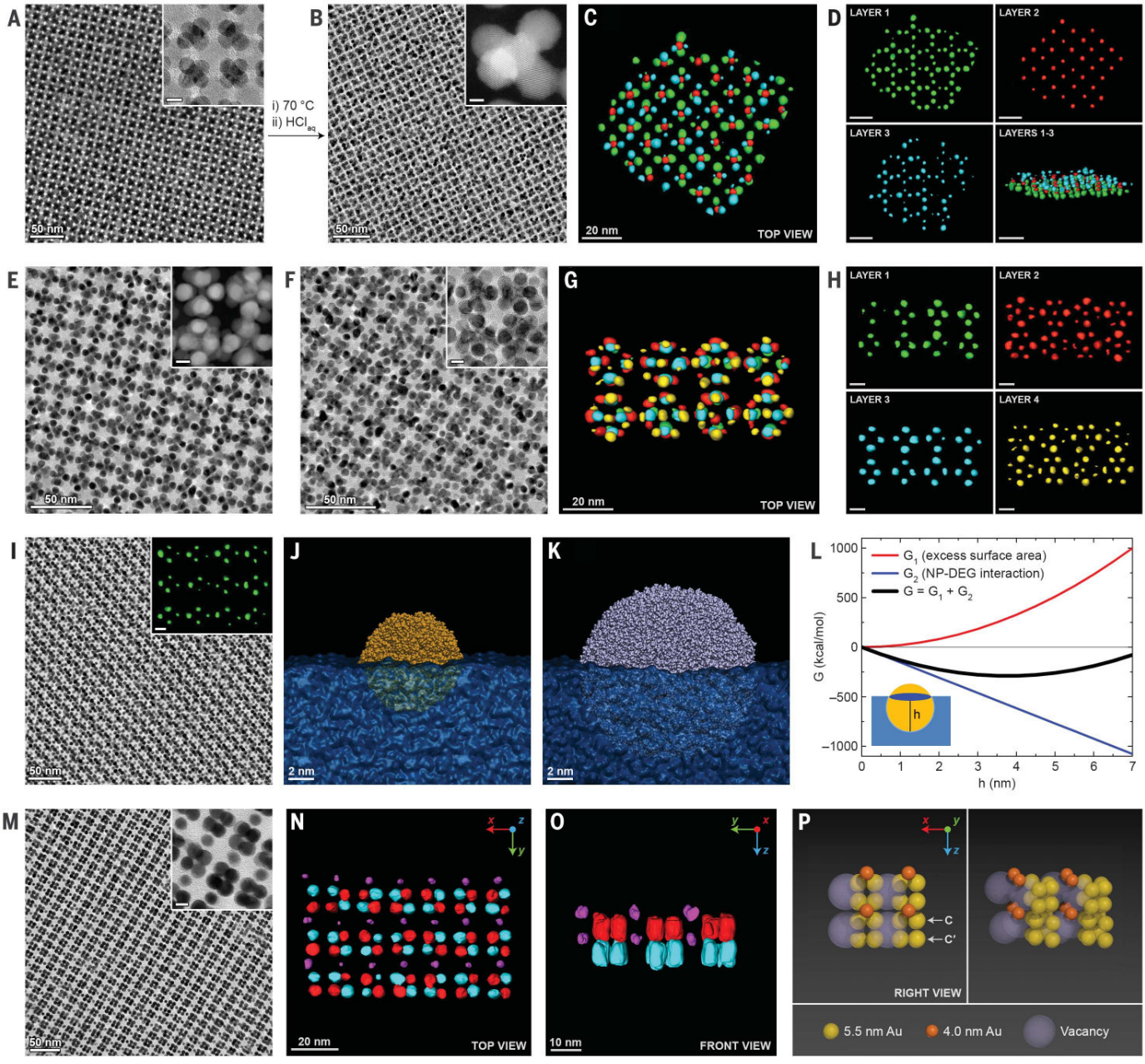


Fig. 2. Structural diversity and characterization of NCP NP arrays. (**A**) TEM image of an AB_6-type BNSL (here, lacking the top layer of Au NPs). (**B**) TEM image of a vac_1Au_5-type array. Scale bar (inset), 2 nm. (**C**) 3D representation of a part of the reconstructed segmented volume of a vac_1Au_5-type array. The different colors correspond to different layers of NPs along the *z* axis. (**D**) Different layers of the vac_1Au_5 array shown separately for clarity. (Bottom right) The structure is tilted by 80° to 85° around the *x* axis. Scale bars, 20 nm. (**E** and **F**) TEM images of vac_1Au_{11}-type arrays terminated with two different layers of Au NPs. (**G**) 3D representation of a part of the reconstructed segmented volume of a vac_1Au_{11}-type array at different viewing directions. (**H**) Four different layers of a vac_1Au_{11}-type array shown separately for clarity. Scale bars, 10 nm. (**I**) TEM image of a $vac_1Au_1Au_2'Au''_1$-type array (Au, Au′, and Au″ denote differently sized Au NPs). (Inset) Bottom layer of $vac_1Au_1Au_2'Au''_1$-type array resolved by means of electron tomography. Scale bar, 10 nm. (**J** and **K**) Atomistic models of (J) a dodecanethiol-functionalized 5-nm Au NP and (K) an oleate-functionalized 10 nm Fe_3O_4 NP relaxed at the DEG-vacuum interface. (**L**) Free energy as a function of immersion height, *h*, for a 5-nm Au NP (protected with a 1-nm-thick ligand shell) immersed into DEG. Red, energy cost to create excess DEG surface area; blue, favorable binding free energy of DEG and Au NP; black, total energy. (**M**) TEM image of a $vac_1Au_1Au'_4$-type array. (**N** and **O**) 3D representation of a part of the reconstructed segmented volume of a $vac_1Au_1Au'_4$-type array at different viewing directions. In (O), entities colored in red and blue all comprise two Au NPs on top of each other. (**P**) Structural model of the $vac_1Au_1Au'_4$-type array. The images in the insets in (B) and (E) have been recorded in HAADF-STEM mode. Scale bars (insets), 5 nm unless indicated otherwise.

by co-assembly of 5.2 nm Au and 10.6 nm Fe_3O_4 NPs premixed in a ~4:1 ratio, in which the thickness of the superlattice depended on the amount of NPs applied at the liquid-air interface. For example, HAADF-STEM tomography revealed that the NCP superlattice shown in Fig. 3B obtained by etching the corresponding BNSL (Fig. 3A) was a hexalayer (Fig. 3C, fig. S43, and database S1) (*19*). Upon extended (>1 hour) heating at 70°C, the original AB_4-type array was transformed into the exotic pattern shown in Fig. 3D (fig. S42) (*19*), whose structure remains

Downloaded from http://science.sciencemag.org/ on October 26, 2017

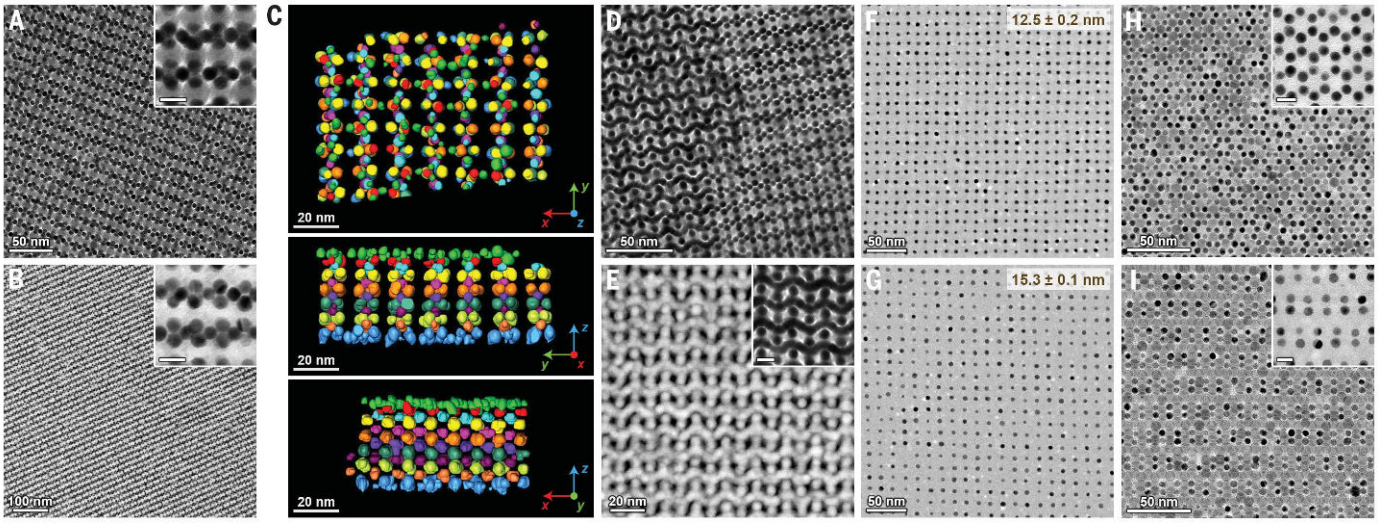


Fig. 3. Extension to multilayers and other nanoparticle sizes. (**A**) TEM image of an AB_4-type binary superlattice. (**B**) TEM image of a vac_1Au_4-type array. (**C**) 3D representation of a part of the reconstructed segmented volume of a hexalayer of a vac_1Au_4-type array at different viewing directions. (**D**) TEM image showing the coexistence of two different types of AB_4 BNSLs and the epitaxial relationship between them. (**E**) HAADF-STEM image of a vac_1Au_4-type array. (**F** and **G**) TEM images of vac_1Au_1-type arrays obtained from BNSLs co-assembled from 5.2-nm Au NPs with (F) 10.6 nm and (G) 13.0 nm Fe_3O_4. (**H**) TEM image of an AB_2-type BNSL and (inset) the corresponding (post-etching) vac_1Au_2-type array. (**I**) TEM image of an A_2B-type BNSL and (inset) the corresponding vac_2Au_1-type array. Scale bars (insets), 10 nm.

to be identified. Detailed theoretical analysis in the supplementary materials confirms that our technique can in principle be extended to NCP arrays having thicknesses approaching macroscopic dimensions (*19*).

Our methodology can also be applied to NP building blocks of other sizes. For example, in Fig. 3, F and G, we extended the average distance between 5.2-nm Au NPs within vac_1Au_1 arrays from 12.5 to 15.3 nm by simply increasing the size of the Fe_3O_4 NPs with which they were co-assembled from 10.6 to 13.0 nm. These results indicate the ability to pattern solid substrates with nanoscopic Au domains, with subnanometer precision. When the sizes of both Au (5.2 nm) and Fe_3O_4 (10.6 nm) NPs were decreased (to 3.0 and 8.4 nm, respectively), many of the BNSLs and the resulting NCP arrays could be recreated on a smaller scale (fig. S45) (*19*). Similarly, working with mixtures of 5.2-nm Au NPs and 8.4-nm Fe_3O_4, we obtained AB-, AB_4-, and ABC_4-type and other BNSLs described above (fig. S46) (*19*). In addition, the modified NP size ratio resulted in novel NP arrays, such as the vac_1Au_2-type and the vac_2Au_1-type structures shown in Fig. 3, H and I (fig. S47) (*19*). The main drawbacks of our method lie in the inherent difficulties in preparing defect-free BNSLs, which limited the size of single-crystalline domains of BNSLs, and hence of NCP arrays, up to several micrometers. In addition, it has proven challenging to control the film thickness throughout the entire area of the sample—for example, a 1:1 mixture of Au and Fe_3O_4 NPs predicted to give rise to a monolayer of the AB-type BNSL afforded a ~20:1:1 mixture of monolayer, bilayer, and noncoated substrate.

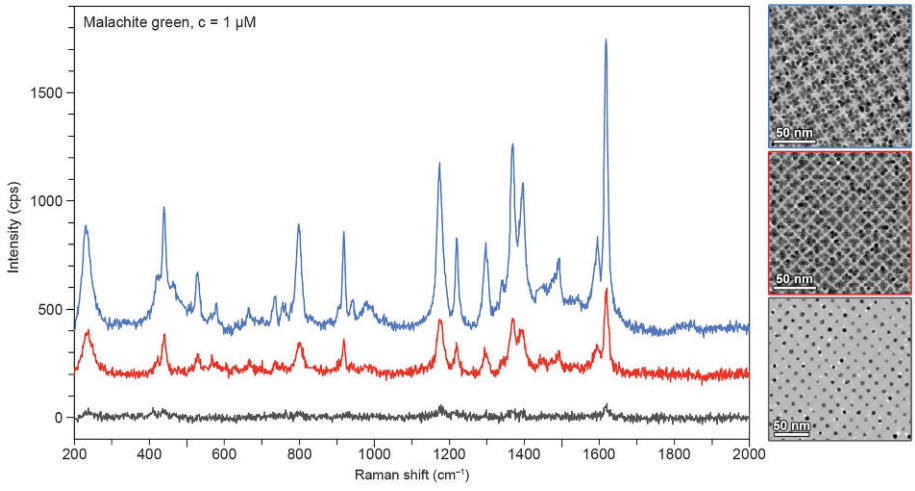


Fig. 4. SERS spectra of a model analyte, malachite green. Spectra were recorded from three different NCP NP arrays shown in the TEM images: vac_1Au_1 (gray), vac_1Au_5 (red), and vac_1Au_{11} (blue).

We envision that NCP NP arrays will have a wide range of interesting optical, mechanical, catalytic, and other properties. As an example, we examined several different NP arrays as substrates for surface-enhanced Raman scattering (SERS) and found that the vac_1Au_{11}-type array has superior signal enhancement properties, as compared with that of vac_1Au_5 (Fig. 4). This is in agreement with a significantly higher density of electromagnetic hotspots at nanometer-sized gaps between NPs within the multilayer structure, into which analyte molecules can readily diffuse through the NCP crystalline lattice (*19*). An attractive avenue will be to use the well-defined nanopores within these materials for trapping active protein molecules. Our procedure leads to surfactant-free Au surfaces, amenable to facile functionalization with thiolated ligands. Our results on multilayers suggest that this method could be readily extended to 3D assemblies, including binary superlattices comprising nonspherical NPs (*28*), quasicrystalline arrays (*29*), and ternary superlattices (*30*).

Downloaded from http://science.sciencemag.org/ on October 26, 2017

REFERENCES AND NOTES

1. E. V. Shevchenko, D. V. Talapin, N. A. Kotov, S. O'Brien, C. B. Murray, *Nature* **439**, 55–59 (2006).
2. N. A. Kotov, F. C. Meldrum, C. Wu, J. H. Fendler, *J. Phys. Chem.* **98**, 2735–2738 (1994).
3. S. Y. Park *et al*., *Nature* **451**, 553–556 (2008).
4. Z. Tang, Z. Zhang, Y. Wang, S. C. Glotzer, N. A. Kotov, *Science* **314**, 274–278 (2006).
5. D. Nykypanchuk, M. M. Maye, D. van der Lelie, O. Gang, *Nature* **451**, 549–552 (2008).
6. G. Singh *et al*., *Science* **345**, 1149–1153 (2014).
7. T. Wang *et al*., *Science* **338**, 358–363 (2012).
8. E. V. Shevchenko *et al*., *J. Am. Chem. Soc.* **130**, 3274–3275 (2008).
9. M. Ibáñez *et al*., *Nat. Commun.* **7**, 10766 (2016).
10. A. Dong, J. Chen, X. Ye, J. M. Kikkawa, C. B. Murray, *J. Am. Chem. Soc.* **133**, 13296–13299 (2011).
11. Y. Kang *et al*., *J. Am. Chem. Soc.* **135**, 42–45 (2013).
12. J. J. Urban, D. V. Talapin, E. V. Shevchenko, C. R. Kagan, C. B. Murray, *Nat. Mater.* **6**, 115–121 (2007).
13. M. P. Boneschanscher *et al*., *Science* **344**, 1377–1380 (2014).
14. H. Lin *et al*., *Science* **355**, 931–935 (2017).
15. A. M. Kalsin *et al*., *Science* **312**, 420–424 (2006).
16. C. J. Kiely, J. Fink, M. Brust, D. Bethell, D. J. Schiffrin, *Nature* **396**, 444–446 (1998).
17. Y. Yu, C. A. Bosoy, D. M. Smilgies, B. A. Korgel, *J. Phys. Chem. Lett.* **4**, 3677–3682 (2013).
18. T. Altantzis, Z. J. Yang, S. Bals, G. Van Tendeloo, M. P. Pileni, *Chem. Mater.* **28**, 716–719 (2016).
19. Materials and methods are available as supplementary materials.
20. A. Dong, J. Chen, P. M. Vora, J. M. Kikkawa, C. B. Murray, *Nature* **466**, 474–477 (2010).
21. Y. Jiao *et al*., *Nat. Commun.* **6**, 6420 (2015).
22. E. V. Shevchenko, D. V. Talapin, C. B. Murray, S. O'Brien, *J. Am. Chem. Soc.* **128**, 3620–3637 (2006).
23. H. Friedrich *et al*., *Nano Lett.* **9**, 2719–2724 (2009).
24. M. P. Boneschanscher *et al*., *Nano Lett.* **13**, 1312–1316 (2013).
25. E. V. Shevchenko, D. V. Talapin, S. O'Brien, C. B. Murray, *J. Am. Chem. Soc.* **127**, 8741–8747 (2005).
26. V. Aleksandrovic *et al*., *ACS Nano* **2**, 1123–1130 (2008).
27. A. Dong, X. Ye, J. Chen, C. B. Murray, *Nano Lett.* **11**, 1804–1809 (2011).
28. X. Ye *et al*., *Nat. Chem.* **5**, 466–473 (2013).
29. Z. Yang, J. Wei, P. Bonville, M. P. Pileni, *J. Am. Chem. Soc.* **137**, 4487–4493 (2015).
30. W. H. Evers, H. Friedrich, L. Filion, M. Dijkstra, D. Vanmaekelbergh, *Angew. Chem. Int. Ed.* **48**, 9655–9657 (2009).

ACKNOWLEDGMENTS

This work was supported by the European Research Council (grants 336080 CONFINEDCHEM to R.K. and 335078 COLOURATOM to S.B.), the Rothschild Caesarea Foundation (R.K.), the NSF (Division of Materials Research, grant 1506886) (P.K.), the European Commission (grant EUSMI 731019 to L.M.L.-M. and S.B.), and the startup funding from the University of Texas at El Paso (L.V.). L.M.L.-M. acknowledges funding from the Spanish Ministerio de Economía y Competitividad (grant MAT2013-46101-R). T.A. acknowledges funding from the Research Foundation Flanders (FWO, Belgium) through a postdoctoral grant. The computer support was provided by the Texas Advanced Computing Center. All data are reported in the main text and supplementary materials.

SUPPLEMENTARY MATERIALS

www.sciencemag.org/content/358/6362/514/suppl/DC1
Materials and Methods
Supplementary Text
Figs. S1 to S52
Tables S1 to S5
Caption for Database S1
References (*31*–*52*)

7 May 2017; accepted 21 September 2017
10.1126/science.aan6046

Downloaded from http://science.sciencemag.org/ on October 26, 2017

Science

Tunable porous nanoallotropes prepared by post-assembly etching of binary nanoparticle superlattices

Thumu Udayabhaskararao, Thomas Altantzis, Lothar Houben, Marc Coronado-Puchau, Judith Langer, Ronit Popovitz-Biro, Luis M. Liz-Marzán, Lela Vukovic, Petr Král, Sara Bals and Rafal Klajn

Science **358** (6362), 514-518.
DOI: 10.1126/science.aan6046

Non–close-packed nanoparticle arrays

Films of colloidal nanoparticles usually form dense, close-packed lattices. If binary lattices could be made and one component removed, then a more open array could form, as long as the remaining nanoparticles could be stabilized. Udayabhaskararao *et al.* formed binary superlattices of gold and magnetite nanoparticles at an air-liquid interface that could then be transferred to carbon-coated surfaces (see the Perspective by Kotov). Selective etching of either of the nanoparticles created non–close-packed arrays with vacancies stabilized by the carbon surface.

Science, this issue p. 514; see also p. 448

ARTICLE TOOLS http://science.sciencemag.org/content/358/6362/514

SUPPLEMENTARY MATERIALS http://science.sciencemag.org/content/suppl/2017/10/26/358.6362.514.DC1

RELATED CONTENT http://science.sciencemag.org/content/sci/358/6362/448.full

REFERENCES This article cites 50 articles, 6 of which you can access for free
http://science.sciencemag.org/content/358/6362/514#BIBL

PERMISSIONS http://www.sciencemag.org/help/reprints-and-permissions

Use of this article is subject to the Terms of Service

Science (print ISSN 0036-8075; online ISSN 1095-9203) is published by the American Association for the Advancement of Science, 1200 New York Avenue NW, Washington, DC 20005. 2017 © The Authors, some rights reserved; exclusive licensee American Association for the Advancement of Science. No claim to original U.S. Government Works. The title *Science* is a registered trademark of AAAS.

Downloaded from http://science.sciencemag.org/ on October 26, 2017